Arabian Journal of Chemistry (2018) xxx, xxx–xxx

King Saud University

Arabian Journal of Chemistry

www.ksu.edu.sa
www.sciencedirect.com

ORIGINAL ARTICLE

Green synthesized SiO_2@OPW nanocomposites for enhanced Lead (II) removal from water

Jyoti Saini [a], **V.K. Garg** [b,*], **R.K. Gupta** [a]

[a] *Department of Chemistry, Guru Jambheshwar University of Science and Technology, Hisar 125001, Haryana, India*
[b] *Centre for Environmental Sciences and Technology, School of Environment and Earth Sciences, Central University of Punjab, Bathinda 155001, Punjab, India*

Received 8 December 2017; accepted 16 June 2018

KEYWORDS

Orange peel waste (OPW);
Silicated orange peel waste (SiO_2@OPW);
Nanoadsorbent;
Adsorption isotherms;
Adsorption kinetics

Abstract The orange peel waste (OPW) was chemically spiked with silica nanospheres, to develop a novel, nanocomposite (SiO_2@OPW) with enhanced adsorption capacity for heavy metals. The dispersion of silica nanospheres into orange peel waste was confirmed by XRD, FTIR, TEM, SEM and EDX. Adsorption of Pb^{2+} ions onto SiO_2@OPW was studied in batch mode under varying process conditions such as pH, metal concentration, contact time and adsorbent dosage. The maximum adsorption capacity for OPW and SiO_2@OPW was 166.7 mg/g and 200.0 mg/g, respectively calculated employing the Langmuir isotherm model. The kinetic data followed pseudo second order and intraparticle diffusion models. The maximum removal of Pb^{2+} ions was at pH = 6.0, adsorbent dosage = 0.02 g/L and contact time 60 min. Regeneration and reusability of SiO_2@OPW was studied for five cycles. Owing to reusability and high adsorption capacity, SiO_2@OPW nanocomposites may be considered as a promising adsorbent for the removal of heavy metals from water and wastewater.

1. Introduction

During the past decades, heavy metals have emerged as a major inorganic pollutant and threat to natural environment and human health. The only solution to protect the environment and human health is their removal from metal laden wastewater before discharging them into aqueous streams. These metal ions, primarily originate from electroplating, mining & ore processing, paint, chemicals and fertilizer industries and metal surface treatment processes (Lawal et al., 2017; Charles et al., 2017; Miranda et al., 2016). Lead is more toxic as compared to several other heavy metals like copper, manganese, zinc and cobalt. Exposure to Pb may cause abdominal pain, neonatal deaths, sterility, damages the nervous system, liver and kidney and affects the process of hemoglobin synthesis, porphyrin metabolism by forming complexes with oxo-groups in enzymes (Charles et al., 2017; Miranda et al., 2016; Rajput et al., 2015). Therefore, it is essential to remove Pb from wastewater before being released into aqueous bodies.

* Corresponding author.
E-mail addresses: vinodkgarg@yahoo.com, vinodkgarg18@gmail.com (V.K. Garg).

Peer review under responsibility of King Saud University.

Production and hosting by Elsevier

https://doi.org/10.1016/j.arabjc.2018.06.003
1878-5352 © 2018 Production and hosting by Elsevier B.V. on behalf of King Saud University.
This is an open access article under the CC BY-NC-ND license (http://creativecommons.org/licenses/by-nc-nd/4.0/).

Please cite this article in press as: Saini, J. et al., Green synthesized SiO_2@OPW nanocomposites for enhanced Lead (II) removal from water. Arabian Journal of Chemistry (2018), https://doi.org/10.1016/j.arabjc.2018.06.003

Several conventional technologies are in use for Pb removal from. These technologies include chemical precipitation, redox approach, ion exchange, electrolysis, membrane separation and adsorption. Amongst these, adsorption is more reliable and promising owing to its efficiency, local availability of adsorbents, operational simplicity, cost effectiveness and regeneration potential of the adsorbents (Musico et al., 2013; Kumar et al., 2014, Joshi et al., 2018, Thitame and Shukla, 2017). Nanoparticles are a new generation of materials emphasized for the environmental remediation due to their unique properties including large surface area, small particle size, pore size, surface charge, thermal stability, magnetic property, chemical inertness and biocompatibility (Ahmed et al., 2015). In yesteryears, several studies have reported the removal of Pb from water and wastewater using nanomaterials. Some of the tested nanomaterials are cross-linked melamine based polyamine/CNT composites (Hamouz et al., 2017), dispersible magnetic chitosan/graphene oxide composites (Fan et al., 2013), EDTA-Fe_3O_4 functionalized with SiO_2 via silanization reaction between N-(trimethoxysilylpropyl) ethylenediamine triacetic acid (Yu et al., 2016). Although these materials are capable to remediate the Pb containing water and wastewater. But it is a challenge to prepare new materials (adsorbents) better in terms of efficiency, environment friendly and cost effective at commercial scale. Various low cost bioadsorbents have been investigated, such as cellulose waste, sawdust, palm-fruits, orange peel, sunflower waste etc. Undoubtly, these adsorbents are economical and available on large scale but they possess low adsorption capacity. Recently attention has been paid to synthesize nanobioadsorbents to improve the adsorption capacity as well as large availability of adsorbent. That is, low cost agricultural waste is modified into nanoscale adsorbents by various physical or chemical techniques. In this study, a novel low cost nanoadsorbent is developed by chemically modified orange peel waste and evaluated its potential as nonadsorbent for the removal of Pb^{2+} ions from aqueous streams. Over the past years, the pristine orange peel has been used to remove metal contaminants of water systems. In this study, silica has been used as a coating material to explore the surface functionality and further enhancing adsorption performance of orange peel waste. Also, comparative adsorption of Pb by pristine orange peel waste (OPW) and silicated orange peel waste (SiO_2@OPW) has been investigated.

2. Experimental section

2.1. Reagents and materials

Orange peels were collected from a food processing industry, India. All other reagents were AR grade and used as such without further purification. The experimental solutions were prepared in double distilled water.

2.2. Synthesis and preparation of the adsorbent

2.2.1. Preparation of dried biomass of orange peel waste

Orange peels were collected from a fruit & vegetable processing industry, washed with double distilled water and dried in oven at 100 °C for 24 h. After that, crushed and sieved through 1.40 mm size sieve and kept in a muffle furnace at 250 °C for 12 h. The powder so obtained was stored in plastic containers for further use.

2.2.2. Preparation of SiO_2 nanoparticles

SiO_2 nanoparticles were prepared by modified Stobber method (Park et al., 2002). 5 mL tetraethoxysilane was added to the absolute ethanol-water 2:1 (v/v) mixture under sonication bath. Then 20 mL of liquor ammonia was dropped slowly into the reaction mixture. The obtained white gel was centrifuged, washed with deionized water and dried in oven at 100 °C for 4 h. Finally fine white nanopowders of SiO_2 nanoparticles was obtained.

2.2.3. Preparation of silicated orange peel waste (SiO_2@OPW) nanocomposites

3.0 g of prepared SiO_2 nanoparticles were dissolved in ethanol-water (1:1) mixture with continuous magnetic stirring at room temperature. Then 15 g of orange peel powder was dispersed in the above reaction mixture. The suspension was stirred for 90 min. and finally transferred to sonication bath for 4 h. The final product SiO_2@OPW was collected by centrifugation, washed and calcined at 200 °C in the muffle furnace.

2.3. Characterization of nanoparticles

The FTIR spectrum was used to identify the functional groups. The IR spectrum of samples was recorded on SHIMADIZU IR AFFINITY-I FTIR spectrophotometer using KBr powder. The crystallinity and crystal structure of SiO_2, OPW and SiO_2@OPWwere analyzed using X-ray diffraction (XRD). XRD patterns of the samples were recorded at room temperature using a Rigaku Miniflex-II diffractometer with Cu K_α radiation in the 2θ range (20–80°) at a scanning rate of 2°/min. Concentration of Pb^{2+} metal ions in solution was determined by atomic absorption spectrophotometer (AAS). The surface morphology, textural structure and elemental composition of samples were obtained by scanning electron microscope (SEM) and energy-dispersive X-ray spectroscopy

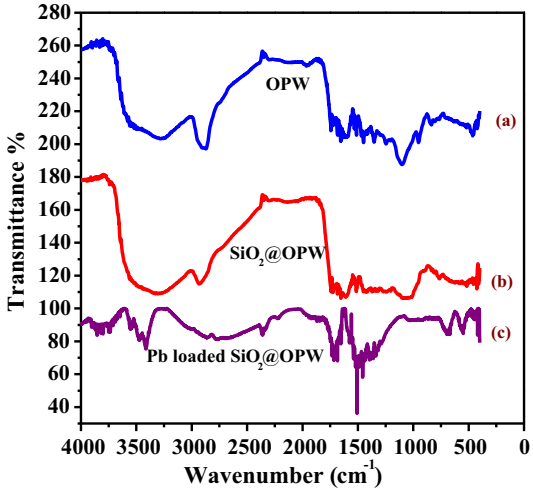

Fig. 1 (a–c) FT-IR spectrum of OPW, SiO_2@OPW and Pb loaded SiO_2@OPW.

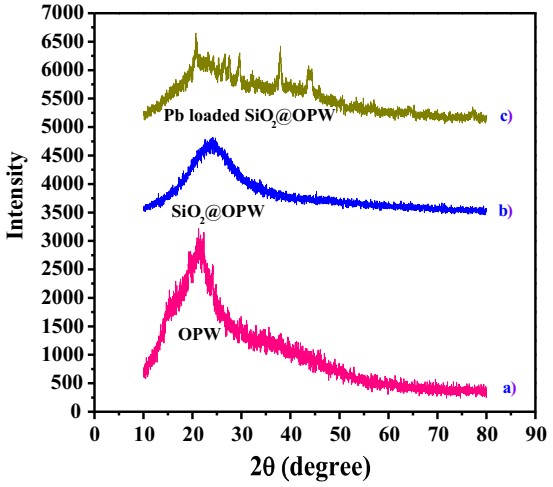

Fig. 2 (a–c) XRD patterns of OPW, SiO_2@OPW and Pb loaded SiO_2@OPW.

(EDX) using Merlin Compact 6073 Scanning Electron Microscope (Carl Zeiss, Germany). Transmission electron microscopy was done to determine the particle size of SiO_2@-OPW by Morgagni 268D (Fei Electron Optics, India).

2.4. Adsorption methods

A stock solution of Pb^{2+} ions (1000 ppm) was prepared in double distilled water using lead nitrate. The adsorption of Pb^{2+} was studied in batch mode experiments under various process conditions like pH, time, concentration, adsorbent dose and adsorbate concentration. Adsorption of Pb^{2+} ions was carried out by shaking known volume of Pb^{2+} solution at constant speed of 180 rpm in a shaker for predetermined time period and then adsorbent was separated by centrifugation. After that, supernatant was used to quantify concentration of Pb^{2+} after the adsorption using Atomic Absorption Spectrophotometer (GBC SensAA). The pH of the solution was adjusted using 0.1 M HCl and 0.1 M NaOH.

The amount of Pb^{2+} ions adsorbed and removal percentage were calculated by the following equations;

$$Metal\ removal(\%) = \frac{(C_o - C_e)}{C_o} \times 100 \quad (1)$$

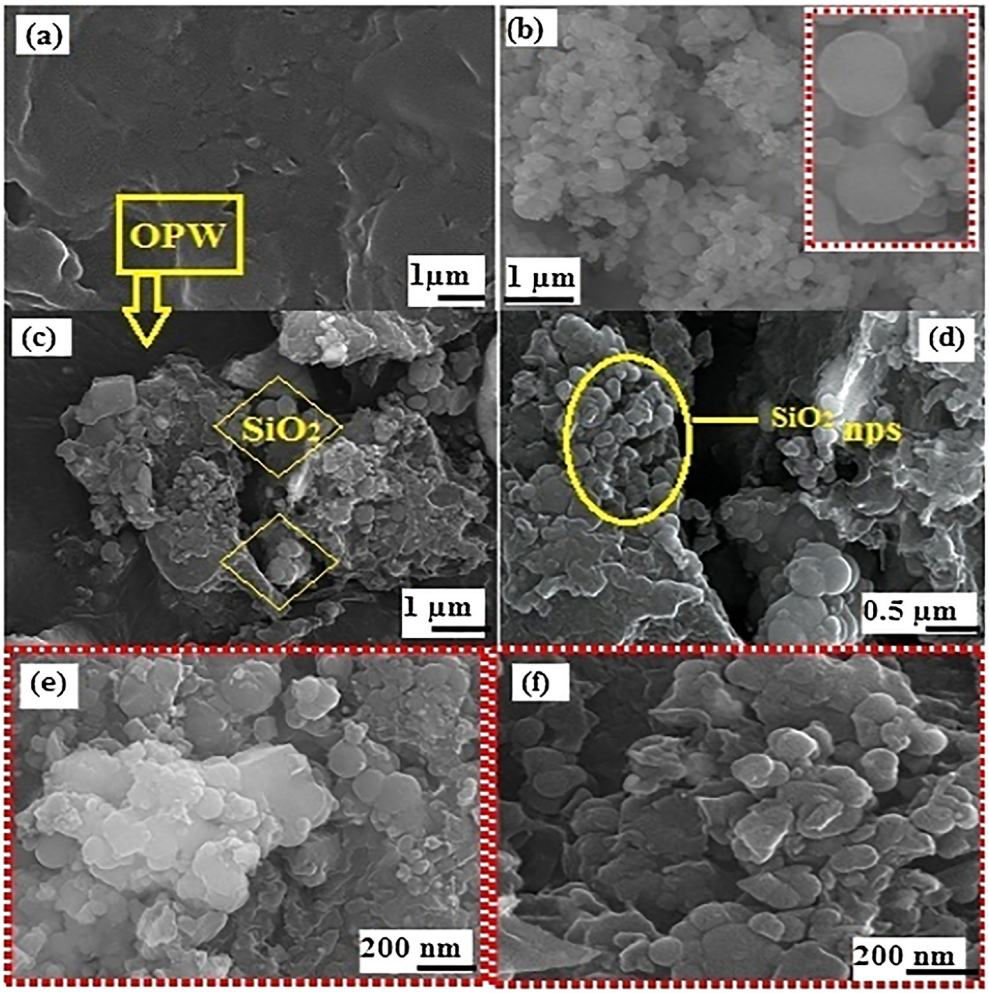

Fig. 3 (a–f) SEM images of (a) OPW (b) SiO_2 and (c–f) SiO_2@OPW.

$$Adsorption\ capacity(q_e) = \frac{(C_o - C_e)V}{m} \quad (2)$$

where C_0 (mg/L) and C_e (mg/L) are the initial and equilibrium concentration of metal ions, respectively, q_e (mg/g) is the amount of Pb^{2+} ions adsorbed onto the adsorbent at equilibrium, V (L) is the volume of solution and m (g) is the mass of adsorbent.

3. Results and discussion

3.1. Characterization of adsorbents

SiO_2@OPW nanocomposites were characterized employing various techniques including FTIR XRD, SEM, EDX and HRTEM.

FTIR spectra of OPW and SiO_2@OPW and Pb^{2+} ions loaded SiO_2@OPW is shown in Fig. 1. The typical absorption band at 3200–3488 cm^{-1} in the FTIR spectrum of OPW may be attributed to —OH groups of carbohydrates, pectin and lignin type polymeric compounds (Fig. 1a). The absorption peak at 2935 cm^{-1} is corresponds to C—H symmetric and asymmetric vibrations and peaks at 1735 cm^{-1} is attributed to carboxylic groups (COOH and $COOCH_3$) (Li et al., 2015; Mafra et al., 2013). The intense peaks appeared at ~1435 cm^{-1} are due to C—H bending vibrations. The signal appeared at 1045 cm^{-1} is due to (C—OH/C—OR) stretching vibrations (Fig. 1a). That absorption peak is becoming somewhat broader in Fig. 1b and almost disappears in Fig. 1c. It may be attributed to the blending of Si—O stretching vibrations in SiO_2@OPW and interactions of Pb^{2+} ions with functional binding sites of SiO_2@OPW Also, an intense signal occurs at 757 cm^{-1} due to Si—O—Si stretching vibrations (Park et al., 2002). Further intensity of absorption peaks in SiO_2@OPW is lesser due to coating of SiO_2 nanospheres over OPW surface. In Fig. 1c, absorption peaks at ~2900 cm^{-1} and 1045 cm^{-1} are vanishing, which indicates the role of C—H and C—OH bonds in adsorption mechanism. New absorption peaks arise at 466 cm^{-1}, 687 cm^{-1} indicate Pb—O and Pb—O—Pb stretching vibrations respectively, which confirms the adsorption of Pb^{2+} ions onto the SiO_2@OPW surface (Arulmozhi et al., 2013).

X-ray spectrum of OPW did not display any distinct peaks at any region. OPW contains completely organic materials having the amorphous nature (Fig. 2a). The broadband at 2θ = 20–30° in Fig. 2b, is attributed to the incorporation of amorphous silica into OPW surface. The diffraction peaks observed at 2θ = 30.8°, 36.6° and 51.8° corresponds to diffraction planes (1 1 1), (2 0 0) and (2 2 0) respectively in the X-ray spectrum of Pb loaded SiO_2@OPW (Fig. 2c) (Theivasanthi and Alagar, 2013). SEM analysis was done to identify the surface texture and morphology of OPW and SiO_2@OPW nanocomposites. The result of SEM analysis is shown in Fig. 3(a)–(f). It can be clearly seen from Fig. 3a that OPW surface is rippled paper like smooth, compact sheet before chemical modification. Fig. 3b shows aggregate spherical silica nanoparticles. Their average particle size distribution is about 12–50 nm. Of course, an obvious agglomeration of silica nanoparticles is observed due to three dimensional hydrophilic networks of —$Si(OH)_2$—O—$Si(OH)_2$— groups onto silica water interface. Aggregate silica nanoparticles distributed on to the surface of the OPW sheet as shown in Fig. 3c and d. Moreover SiO_2 nanospheres completely covered the wrinkled paper like sheet of the OPW and provides different functional binding sites (—Si—O—Si—, Si—O^-) for adsorption of Pb^{2+} ions (Fig. 3e and f) (Saini et al., 2018). Fig. 4(a)–(d) gives the

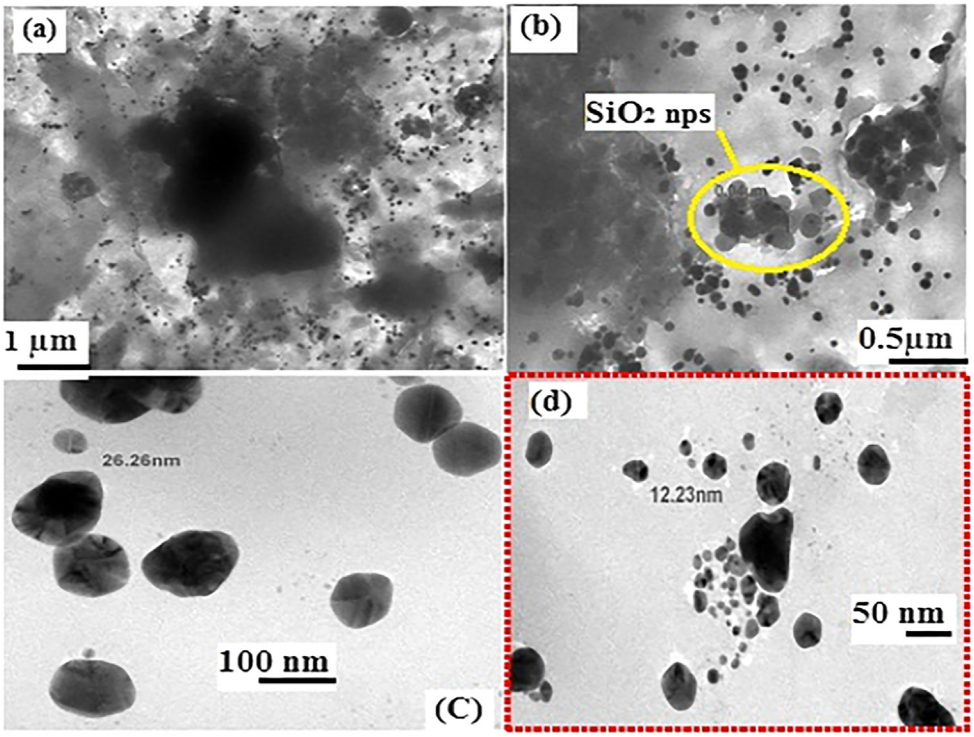

Fig. 4 (a–d) TEM images of SiO_2@OPW.

corresponding TEM images of SiO_2@OPW nanospheres. These images also confirmed the spherical shape of silica nanoparticles and their continuous entrapping into the OPW surface (Fig. 4a and b). The average particle size of SiO_2@OPW nanocomposites is about 26–200 nm as shown in TEM images.

EDX analysis has been done to find out the elemental composition of OPW, SiO_2@OPW and Pb loaded SiO_2@OPW before and after adsorption of Pb^{2+} ions. The weight percent of the detected elements in OPW is C 66.88, O 35.85, Si 0.62 and some additional peaks of copper and silver also appears (Fig. 5a). The weight percent of C 54.79, O 35.58 and Si 9.27 in SiO_2@OPW is evident from Fig. 5b. Further weight percent of C 56.19, O 35.58, Si 1.27 and Pb 5.38 is observed in the EDX spectrum of Pb^{2+} loaded SiO_2@OPW indicates adsorption of Pb^{2+} ions. Meanwhile, decrease in peak intensity of silica indicates participation of functional binding sites of silica in the adsorption mechanism (Fig. 5c).

3.1.1. Mechanism of adsorption

Uptake of Pb^{2+} ions onto SiO_2@OPW is understood in terms of (a) Colloidal suspension surface charge; (b) Surface complexation of Pb^{2+} with different functional groups like COOH, OH and C═O present into pectin, lignin and cellulose of OPW; (c) Surface precipitation and physical adsorption. COO^- sites present in pectin creates chelation with Pb^{2+} ions. COOH and O—H groups are involved in ion exchange between Pb^{2+} and O^- sites. Polymeric chains of silica hydrogel produce three dimensional network of —$Si(OH)_2$—O—$Si(OH)_2$— groups onto silica water interface. This three dimensional network of $Si(OH)_2$—O—$Si(OH)_2$ is hydrophilic and capable of holding a large number of [SiO^-] sites. Colloidal interactions of silica hydrogel are primarily strong vander wall interactions with the adsorbate species. These additional anionic binding sites introduce electrostatic attractions between Pb^{2+}, [Si—O^-] and [—Si—O—Si—]. In addition, Pb^{2+} is co-precipitated as Pb$(OH)_2$, Pb$(CO_3)_2$ and Pb$(SiO)_3$ in alkaline metallic solution. Meanwhile, decrease in peak intensity of silica (9.27–1.27) in the EDX spectrum of Pb^{2+} loaded SiO_2@OPW confirms participation of functional binding sites of silica in the adsorption of Pb^{2+} (Mei et al., 2015; Yang et al., 2015; Shao et al., 2012). All possible interactions of Pb^{2+} onto SiO_2@OPW are schematically illustrated in Scheme 1.

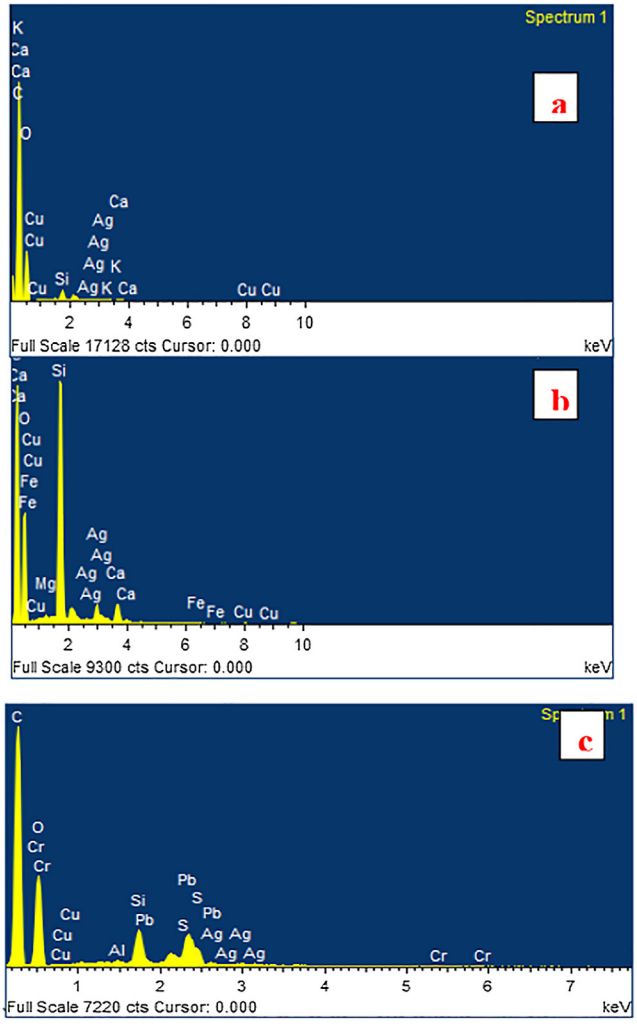

Fig. 5 (a–c) EDX of OPW, SiO_2@OPW and Pb loaded SiO_2@OPW.

3.2. Adsorption experiment

3.2.1. Effect of pH

The affinity of adsorbent functional sites for metallic ions depends on the initial pH of the adsorbate solution. Lead occurs as Pb^{2+}, $Pb(OH)^+$ and $Pb(OH)_2$ species in deionized water. Typically, Pb^{2+} ions exist in the 6.5 pH solution, afterward, in the pH range from 6.5 to 9.0 exist as $Pb(OH)^+$. The effect of pH on adsorption of Pb^{2+} ions was studied over a pH range of 2.0–8.0. The adsorption capacity for Pb^{2+} ions of both the adsorbents increased sharply from pH 2 to 6. Further the adsorption of Pb^{2+} reduced below pH 2.0 and above pH 6.0. Precipitation occurs at higher pH as Pb^{2+} ions precipitate as $Pb(OH)^+$, $Pb(OH)_2$, and $Pb(OH)_3$. The Similar observations have been reported for the adsorption of Pb^{2+} ions by other authors (Kumar et al., 2014; Miranda et al., 2016).

Actually, in acidic solutions too H^+ ions concentration is not significant for replacement of Pb^{2+} ions is being attributed to competitive adsorption between proton and Pb^{2+} ions for occupying active sites onto OPW and SiO_2@OPW. May be functional groups on the adsorbents protonated and caused electrostatic repulsion for Pb^{2+} ions (Kataria and Garg, 2018). In the alkaline range electrostatic attractions occur between cationic Pb^{2+} ions and anionic adsorbent surface. This may be attributed to the deprotonation of functional groups like carboxylic (COOH) as COO^-, alcohols and phenols (OH) as O^- and SiOH as Si—O^- at higher pH. The percent removal of Pb^{2+} increased from 21.82% to 88.22% by OPW and 26.58% to 95.86% by SiO_2@OPW (Fig. 6a).

3.2.2. Effect of adsorbent dose on Pb^{2+} adsorption

The influence of adsorbent dose on the removal of Pb^{2+} was studied by varying the adsorbent dose from 0.01 g/50 mL to 0.03 g/50 mL. Percent removal of Pb^{2+} increased from 62.76% to 88.96%, 68.82% to 98.02% respectively onto OPW and SiO_2@OPW with an increase in adsorbent dose (Fig. 6b). This may be due to increase in adsorption sites and surface area due to increase in adsorbent dose. These results for Pb^{2+} ion removal are in agreement with the findings of other authors (Miranda et al., 2016; Ay et al., 2017; Saini

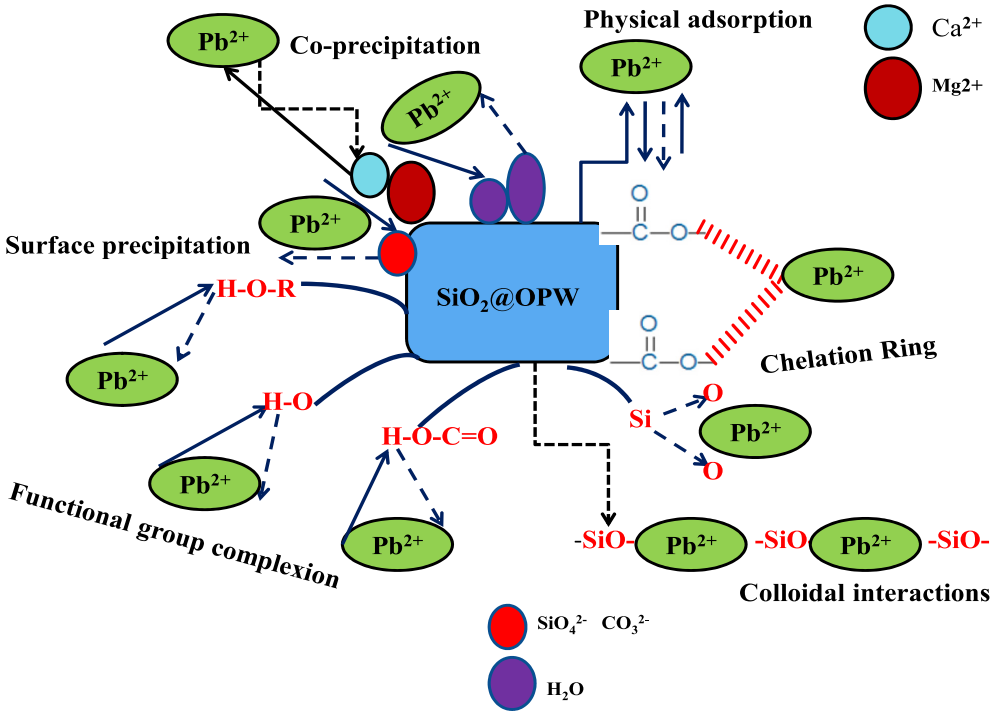

Scheme 1 Possible interactions between SiO_2@OPW and Pb^{2+} ions.

et al., 2017). On the other hand, the adsorption capacity of OPW and SiO_2@OPW decreased from 156.90 to 74.13 mg/g and 172.05 to 81.68 mg/g respectively with increase in the adsorbent dose. SiO_2@OPW has more adsorption capacity than OPW that may be due to availability of more functional binding sites on the SiO_2@OPW surface.

3.2.3. Effect of contact time and Pb^{2+} concentration on Pb^{2+} adsorption

The effect of contact time and Pb^{2+} concentration is depicted in Fig. 7. The experiments were performed by varying contact time (10–60 min.) and initial Pb^{2+} concentration (10–100 mg/L) keeping all other parameters constant. The percent removal increased from 58.68% to 87.88% onto OPW and 63.43% to 93.94% onto SiO_2@OPW with time. Herein, the adsorption capacities of OPW increased from 22.03 to 147.38 mg/g and adsorption capacity of SiO_2@OPW increased 24.92 to 197.93 mg/g as the initial concentration of Pb^{2+} ions increased from 10 to 100 mg/g. These results suggested that the actual amount of Pb^{2+} ions adsorbed per unit mass of the adsorbent increased with metal ion concentration (Ay et al., 2017; Ilangovan et al., 2017; Luo et al., 2016).

3.2.4. Effect of temperature on Pb^{2+} adsorption

The effect of temperature on the adsorption of Pb^{2+} was studied by varying temperature in the range of 10–50 °C. The Pb^{2+} adsorption increased from 43.98% to 93.94% onto OPW and 52.72% to 97.36% onto SiO_2@OPW with increase in temperature (Fig. 8). The adsorption capacities also increased from 54.98 to 117.43 mg/g and 65.9 to 121.7 mg/g onto OPW and SiO_2@OPW respectively. This may be due to increased mobility of ions with rise in temperature and increase in the number of adsorptive sites due to adsorbent rupture at higher temperature. The adsorption of Pb^{2+} ions may be endothermic in nature as the adsorption percentage increased with temperature (Lawal et al., 2017; Luo et al., 2016).

3.3. Equilibrium isotherms

To better analyze the equilibrium relationship between Pb^{2+} and SiO_2@OPW, the equilibrium data was modeled by two common models, viz., the Langmuir isotherm model and the Freundlich isotherm model. These adsorption isotherms provide the adsorption capacity of adsorbents in order to choose the efficient adsorbents for water treatment and also to compare the adsorption capacities of various adsorbents. The Langmuir equilibrium isotherm model assumes monolayer distribution of metal ion concentration at specific homogeneous sites within the adsorbent surface and no interaction between adsorbed species. While the Freundlich isotherm model describes that adsorption happens on the heterogeneous surface system. The isotherm model provides the relationship between the amount of adsorbate adsorbed per unit mass of the adsorbent and concentration of adsorbate at equilibrium.

Linear forms of Langmuir and Freundlich isotherm are given in Eqs. (3) and (4) respectively (Langmuir, 1918; Freundlich, 1906).

$$\frac{C_e}{q_e} = \frac{1}{q_{max} b} + \frac{C_e}{q_{max}} \quad (3)$$

$$log q_e = log K_f + \frac{1}{n} log C_e \quad (4)$$

where q_{max} (mg/g) is the maximum adsorption capacity at monolayer coverage, b (L/mg) is the Langmuir constant

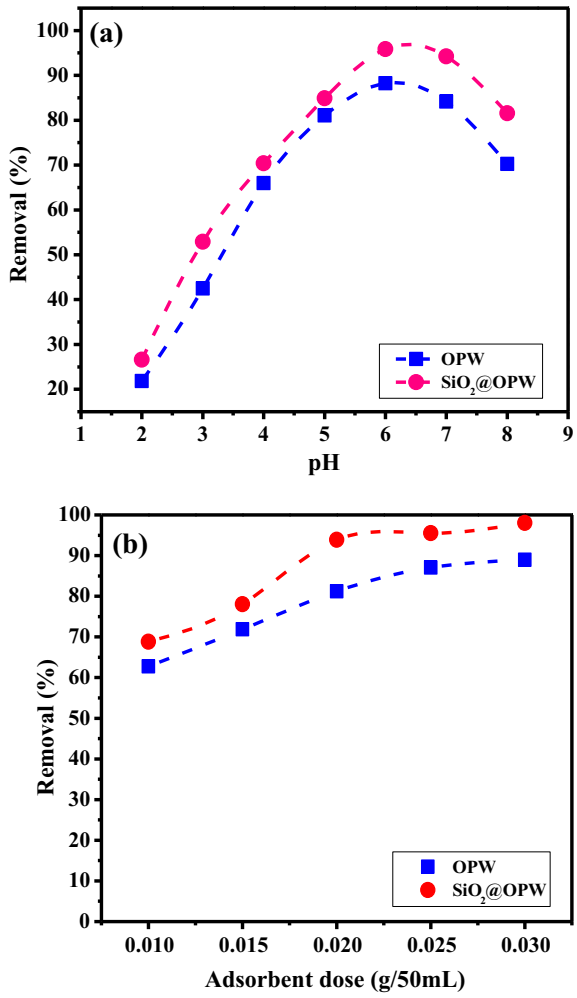

Fig. 6 (a) Effect of pH on adsorption of Pb^{2+} ions onto OPW and SiO_2@OPW (Experimental Conditions: Pb^{2+} conc. – 50 mg/L, adsorbent dose – 0.02g/50mL, temp. – 27 °C, contact time – 1 h). (b) Effect of adsorbent dose on adsorption of Pb^{2+} ions onto OPW and SiO_2@OPW nanocomposites. (Experimental Conditions: pH – 6, Pb^{2+} ions conc. – 50 mg/L, temp. – 27 °C, contact time – 1 h).

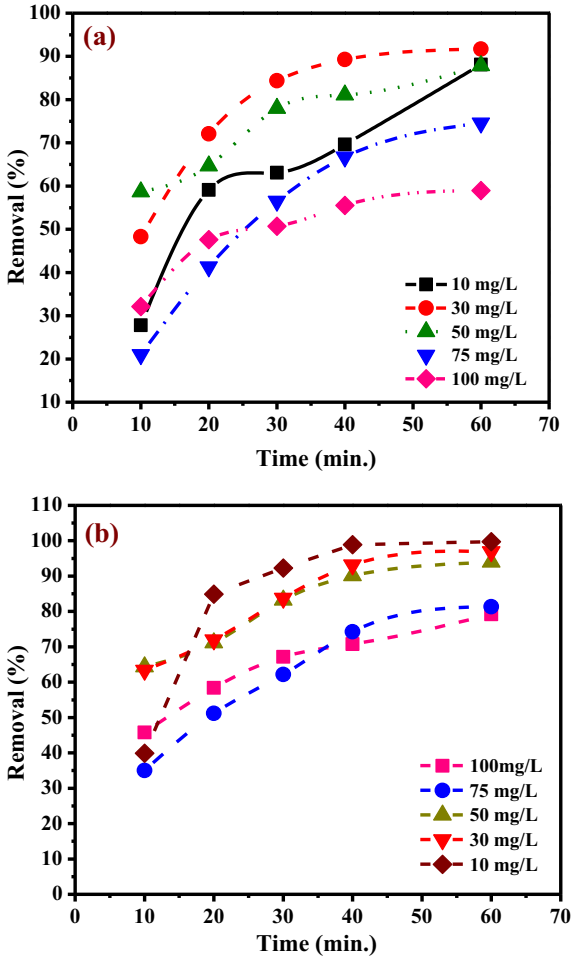

Fig. 7 (a) Effect of metal ion concentration and contact time on Pb^{2+} adsorption onto OPW (b) Onto SiO_2@OPW. (Experimental Conditions: Pb^{2+} ion conc.: 10–100 mg/L, temp.: 27 °C, contact time: 1 h, pH: 6.0).

parameter related to the energy of adsorption and affinity of binding sites between adsorbate and adsorbent. K_f is Freundlich constant. The constant n, is the heterogeneity factor related to the intensity and favorability of the adsorption. The value of q_{max} (mg/g), b (L/mg) and correlation coefficient (R^2) are determined from a plot of C_e/q_e v$_s$ C_e (Fig. 9a and b). The constant K_f, R^2 and n are calculated from the slope and intercept of the plot between log q_e and log C_e (Fig. 10a and b). The values of n should lie in between 1 and 10 for favourable adsorption. All the calculated parameters are listed in Table 2.

Here, the value of the correlation coefficient R^2 for Langmuir isotherm was (0.999) for both OPW and SiO_2@OPW and the adsorption capacity was 166.6 mg/g, 200.0 mg/g onto OPW and SiO_2@OPW which is much closer to the experimental results i. e. 147.37 mg/g and 197.93 mg/g. The value of coefficient R^2 was 0.952 and 0.929 for OPW and SiO_2@OPW as

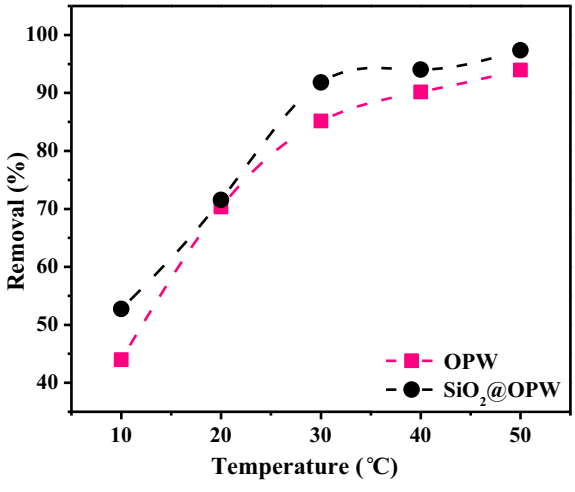

Fig. 8 Effect of temperature on the adsorption of Pb^{2+} ions onto OPW and SiO_2@OPW. (Experimental Conditions: pH – 6, metal ion conc. – 50 mg/L, dose – 0.02 g/50 mL, contact time – 1 h).

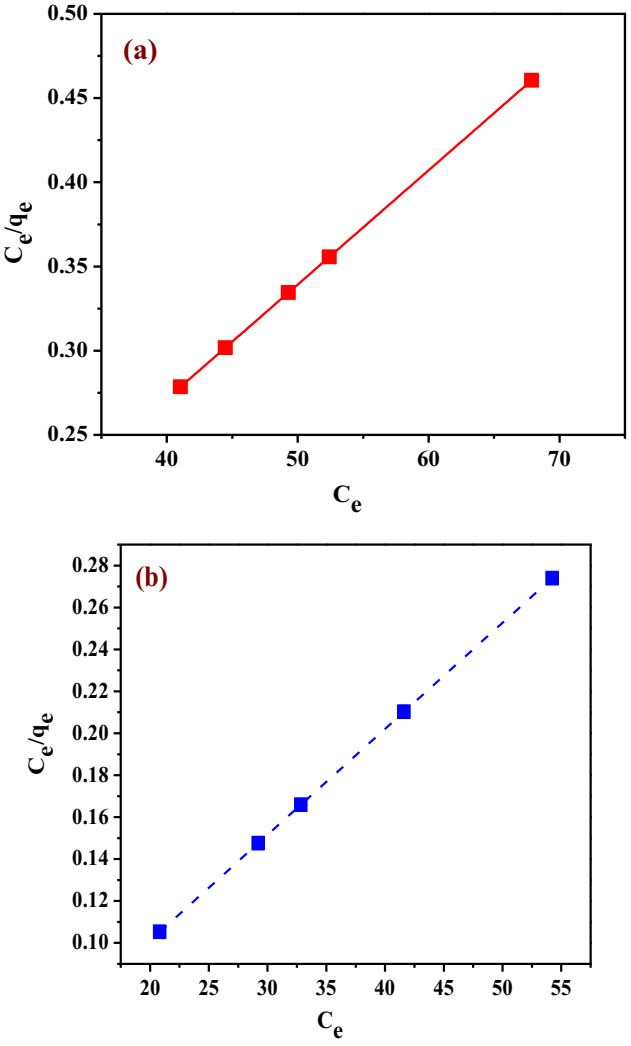

Fig. 9 Langmuir adsorption isotherms plots for Pb^{2+} ions onto OPW and SiO_2@OPW (a) OPW, (b) SiO_2@OPW.

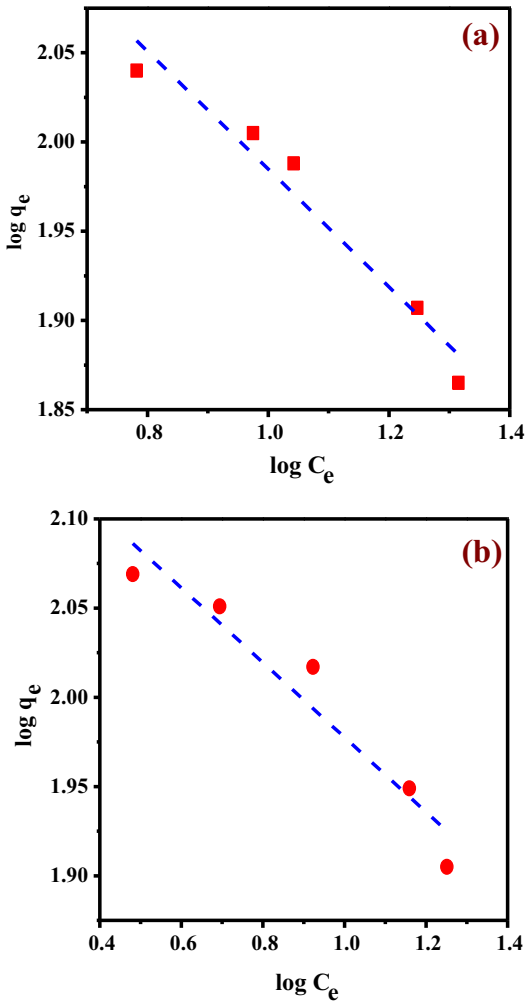

Fig. 10 Freundlich adsorption isotherm plot for Pb^{2+} metal ions onto OPW and SiO_2@OPW (a) OPW, (b) SiO_2@OPW

obtained from Freundlich isotherm. In comparison to Freundlich isotherm, owing to high values of correlation coefficients and adsorption capacities the Langmuir isotherm fits better with the experimental data for Pb^{2+} adsorption onto SiO_2@OPW. The calculated adsorption capacity was much higher than the other previously reported studies [Table 3].

3.4. Adsorption kinetics

To investigate the rate mechanism the, experimental data was evaluated by pseudo-first order, pseudo-second order and intraparticle diffusion equations given as Eqs. (5–7) respectively (Lagergren, 1898; Ho and Mckay, 1999; Weber and Morris, 1963).

$$\log(q_e - q_t) = \log q_e - \left(\frac{k_1}{2.303}\right)t \tag{5}$$

$$\frac{t}{q_t} = \frac{1}{k_2 q_e^2} + \frac{t}{q_e} \tag{6}$$

$$q_t = k_{id}t^{1/2} + C \tag{7}$$

where q_e and q_t (mg/g) are the amount of Pb^{2+} adsorbed per unit mass of the adsorbent at any time t and equilibrium time, respectively, k_1 (min^{-1}) and k_2 (g mg^{-1} min^{-1}) are the pseudo-first order and pseudo-second order rate constants, k_{id} is the intraparticle diffusion rate constant and C is intercept which provides an approximation about the thickness of the boundary layer. k_1 and q_e is calculated from the slope and intercept of a linear plot between log ($q_e - q_t$) and t (Figs. 11 and 12a). The equilibrium capacity, q_e and k_2 is determined from the slope and intercept of the plot between t/q_t versus t as shown in Figs. 11 and 12b. The value of C and k_{id} can be obtained by the slope and intercept of the plot between $t^{1/2}$ versus q_t (Figs. 11 and 12c). The calculated parameters were listed in Table 1.

A better straight line fitting, correlation coefficient R^2 (>0.999) is obtained for both OPW and SiO_2@OPW from pseudo-second order equation. Meanwhile the calculated q_e values are in good agreement with experimental q_e values. These results confirmed the well fitting of Pseudo-second-order equation for the adsorption of Pb^{2+} onto SiO_2@OPW.

Table 1 Kinetic models parameters study for Pb^{2+} ion uptake onto OPW and SiO_2@OPW.

		Values of parameters			
		OPW		SiO_2@OPW	
Kinetic models parameters		50 mg/L	100 mg/L	50 mg/L	100 mg/L
Pseudo-first order	k_1 (min^{-1})	0.071	0.080	0.085	0.073
	q_e (cal)	0.304	0.351	0.394	0.305
	R^2	0.953	0.972	0.904	0.978
Pseudo-second order	k_2 (g/mg min)	0.0004	0.0009	0.00033	0.00081
	q_e (cal)	125.0	200.0	142.85	250.0
	R^2	0.994	0.997	0.995	0.997
Intraparticle diffusion	k_{id} (mg g^{-1} $min^{-1/2}$)	9.63	16.33	10.08	20.58
	C	41.48	35.87	47.23	51.50
	R^2	0.969	0.936	0.980	0.988
Experimental data	q_e (exp)	109.85	147.37	117.43	197.0

Intraparticle diffusion plot uptake is linear, which indicates its participation in the adsorption kinetics of Pb^{2+} onto SiO_2@OPW (Zhu et al., 2018). Although, it did not pass through the origin, confirms not only intraparticle diffusion is a rate limiting step but other kinetic models also. Based on that interpretation, adsorption of Pb^{2+} ions onto SiO_2@OPW is a complex diffusion process involving both boundary layer diffusion and intraparticle diffusion.

Table 2 Adsorption isotherms model parameters for Pb^{2+} ions uptake onto OPW and SiO_2@OPW.

Isotherms model	Parameters	Parameters values	
		OPW	SiO_2@OPW
Langmuir	q_{max} (mg/g)	166.6	200
	b (L/mg)	0.006	0.005
	R^2	0.999	0.999
Freundlich	1/n	3.03	4.78
	K_f (mg/g)	2.314	2.186
	R^2	0.953	0.929

3.4.1. Desorption and reuse potential of SiO_2@OPW

Adsorbed Pb^{2+} ions were removed from metal laden SiO_2@-OPW using hydrochloric acid of various strengths ranging from 0.1 to 0.3 M. 0.03 g of metal amalgamated SiO_2@OPW were added to 20 mL of HCl of desired concentration and agitated for 60 min in a closed shaker. Desorption efficiency was increased from 48.3% to 82.5% with increasing HCl concentration. Existance of H^+ sites at lower pH favours the regeneration of SiO_2@OPW. However an optimum was achieved at 0.025 M, further on desorption efficiency remained constant. Five adsorption-desorption cycles were evaluated to determine the reuse potential of SiO_2@OPW. The results showed that SiO_2@OPW nanoadsorbents had good removal efficiency (80.16–85.62%) upto three cycles. The removal efficiency was ~68.9% during 4th and 5th cycle (Fig. 13).

Table 3 Adsorption capacity of various adsorbents for Pb^{2+} ion.

Adsorbent	$q_{max.}$ (mg/g)	Reference
Nitrogen functionalized mesoporous Carbon	80.42	Yang et al. (2014)
Nanocomposite of ZnO with Montmorillonite	88.05	Sani et al. (2018)
Ethylenediamine-modified yeast biomass mixed matrix membrane	121.26	Li et al. (2013)
Polysulfone/hydrous ferric oxide	13.20	Abdullah et al. (2016)
Mixed membrane		
Activated carbon prepared from rapeseed oil	133.8	Erdem et al. (2015)
Graphene oxide-hydrated manganese oxide nanocomposites	500.0	Wan et al. (2016)
Magnetic cellulose nanocomposite beads entrapping activated bentonite	12.6	Luo et al. (2016)
Black walnut (*Juglan nigra*) husk	3.0	Lawal et al. (2017)
	115	
Nanoscale zero valent supported by Zeolite and Montmorillonite	115 and 50.3	Miranda et al. (2016)
Pine cone activated carbon	27.53	Momcilovic et al. (2011)
OPW	166.6 Present work	
SiO_2@OPW	200.0 Present work	

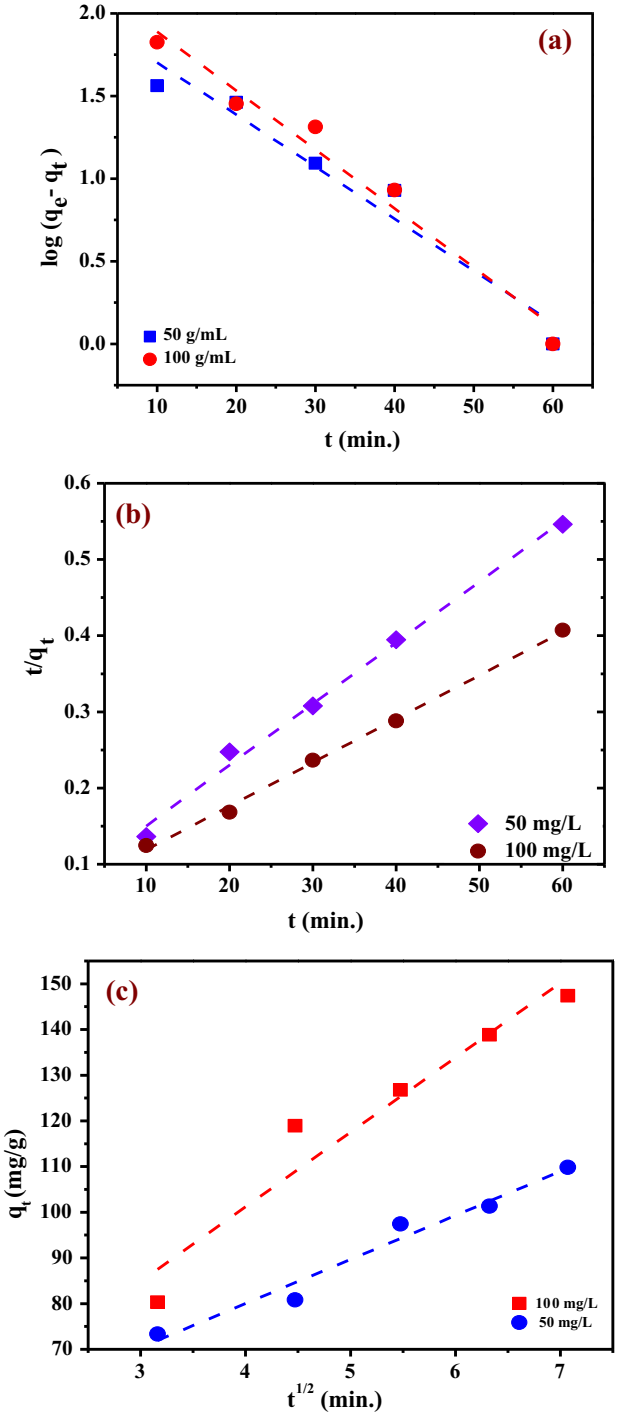

Fig. 11 Kinetic plots for adsorption for Pb^{2+} metal ions onto OPW. (a) Pseudo-first-order plot, (b) pseudo-second order plot, (c) intraparticle diffusion plot.

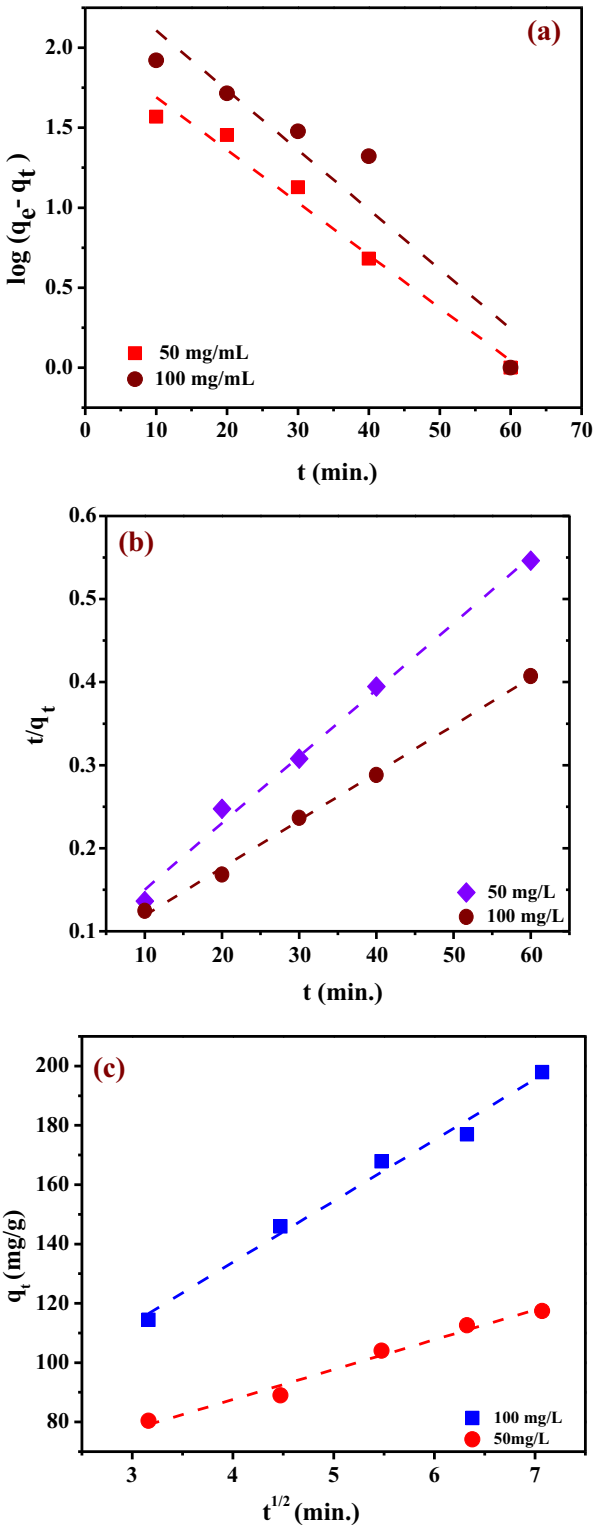

Fig. 12 Kinetic plots for adsorption for Pb(II) metal ions onto SiO_2@OPW. (a) Pseudo-first-order plot, (b) pseudo-second-order plot, (c) intraparticle diffusion plot.

4. Conclusion

A novel adsorbent, SiO_2 functionalized orange peel waste (SiO_2@OPW) has been prepared, characterized & tested for Pb^{2+} adsorption from aqueous medium to explore its potential in wastewater treatment. The dispersion of SiO_2 onto the surface of OPW is confirmed by XRD, FTIR, SEM and TEM images. SiO_2@OPW has enhanced adsorption capacity for Pb^{2+} ions as compared to pristine orange peel waste. Increase in adsorption capacity of SiO_2@OPW may be attributed to new electrostatic interactions between Pb^{2+}, Si—O^-

Please cite this article in press as: Saini, J. et al., Green synthesized SiO_2@OPW nanocomposites for enhanced Lead (II) removal from water. Arabian Journal of Chemistry (2018), https://doi.org/10.1016/j.arabjc.2018.06.003

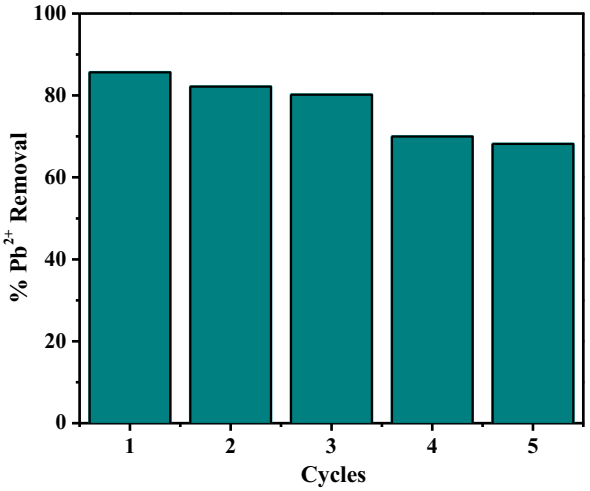

Fig. 13 Efficiency of SiO_2@ OPW for Pb^{2+} removal during adsorption–desorption cycles.

and —Si—O—Si— functional binding sites of SiO_2 nanospheres entrapped onto the OPW. The optimum adsorbent dosage was 0.02 g/L at pH = 6. The maximum monolayer adsorption capacity calculated from Langmuir isotherm model was 166.6 mg/g, 200.0 mg/g for OPW and SiO_2@OPW respectively. The kinetic data fitted well to the pseudo-second-order and intraparticle diffusion models.

References

Abdullah, N., Gohariac, R.J., Yusof, N., Ismail, A.F., Juhana, J., Lau, W.J., Matsuura, T., 2016. Polysulfone/hydrous ferric oxide ultrafiltration mixed matrix membrane: preparation, characterization and its adsorptive removal of lead (II) from aqueous solution. Chem. Eng. J. 289, 28–37.

Ahmed, Y.M., Al-Mamun, A., Khatib, M.R., Al, JameelA.T., AlSaadi, M., 2015. Efficient lead sorption from wastewater by carbon nanofibers. Environ. Chem. Lett. 13, 341–346.

Arulmozhi, K.T., Mythili, N., 2013. Studies on the chemical synthesis and characterization of lead oxide nanoparticles with different organic capping agents. AIP Adv. 3, 122.

Ay, C., Ozcan, A., Erdogan, Y., Ozcan, A., 2017. Characterization and lead(II) ions removal of modified Punica granatum L. peels. Int. J. Phytoremediation 19, 327–339.

Charles, O., Hamouz, A., Estatie, M.K., Morsy, M.A., Saleh, T.A., 2017. Lead ion removal by novel highly cross-linked Mannich based polymers. J. Taiwan Inst. Chem. Eng. 70, 345–351.

Erdem, M., Tay, T., Karago, S., Ucar, S., 2015. Removal of lead (II) and nickel (II) ions from aqueous solution using activated carbon prepared from rapeseed oil cake by Na_2CO_3 activation. Clean Technol. 17, 747–756.

Fan, L., Luo, C., Sun, M., Li, X., Qiu, H., 2013. Highly selective adsorption of lead ions by water-dispersible magnetic chitosan/graphene oxide composites. Colloids Surf. B 103, 523–529.

Freundlich, H., 1906. Uber die adsorption in lasugen. J. Phys. Chem. 57, 385–470.

Hamouz, O.C.S.A., Adelabu, I.O., Saleh, T.A., 2017. Novel cross-linked melamine based polyamine/CNT composites for lead ions removal. J. Environ. Manage. 192, 163–173.

Ho, Y.S., Mckay, G., 1999. Pseudo-second order model for sorption processes. Biochem 34, 451–465.

Ilangovan, M., Guna, V., Olivera, S., Ravi, A., Muralidhara, H.B., Santosh, M.S., Reddy, N., 2017. Highly porous carbon from a natural cellulose fiber as high efficiency sorbent for lead in waste water. Bioresource Technol. 245, 296–299.

Joshi, S., Garg, V.K., Saini, J., Kadirvelu, K., 2018. Removal of toulidine blue O dye from aqueous solution by silica-iron oxide nanoparticles. Mater. Focus. 7, 140–146.

Kataria, N., Garg, V.K., 2018. Green synthesis of Fe_3O_4 nanoparticles loaded sawdust carbon for Cadmium (II) removal from water: regeneration and mechanism. Chemosphere 208, 818–828.

Kumar, S., Nair, R.R., Pillai, P.B., Gupta, S.N., Iyengar, M.A.R., Sood, A.K., 2014. Graphene oxide–$MnFe_2O_4$ magnetic nanohybrids for efficient removal of lead and arsenic from water. Appl. Mater. Interf. 6, 7426–17436.

Lagergren, S., 1898. About the theory of so-called absorption of soluble substances. Kunglia Svenska Vetenskapsakademiens Handlingar 24, 1–3.

Langmuir, I., 1918. The adsorption of gases on plane surfaces of glass, mica and platinum. J. Am. Chem. Soc. 40, 1361–1403.

Lawal, O.S., Ayanda, O.S., Rabiu, O.O., Adebowal, K.O., 2017. Application of black walnut (Juglan) husk for the removal of ion from aqueous solution. Water Sci. Technol. 75, 2454–2464.

Li, T., Liu, Y., Peng, Q., Hua, X., Liao, T., Wang, H., Lu, M., 2013. Removal of lead(II) from aqueous solution with ethylenediamine-modified yeast biomass coated with magnetic chitosan microparticles: kinetic and equilibrium modeling. Chem. Eng. J. 214, 189–197.

Li, P., Xia, J., Shan, Y., Niel, Z., Wang, F., 2015. Effects of surfactants and microwave-assisted pretreatment of orange peel on extracellular enzymes production by aspergillus japonicas. Appl. Biochem. Biotechnol. 176, 758–771.

Luo, X., Lei, X., Xie, X., Yu, B., Cai, N., Yu, F., 2016. Adsorptive removal of Lead from water by the effective and reusable magnetic cellulose nanocomposite beads entrapping activated bentonite. Carbohyd. Polym. 151, 640–648.

Mafra, M.R., Mafra, L., Zuim, D.R., Vasques, É.C., Ferreira, M.A., 2013. Adsorption of remazol brilliant blue on an orange peel adsorbent. Braz. J. Chem. Eng. 30, 657–665.

Mei, H., Yu, S., Tan, X., Wang, S., Chen, C., Li, J., 2015. Evaluation of the influence of environmental conditions on the removal of Pb (II) from wastewater by Ca-rectorite. Sep. Sci. Technol. 50, 2257–2266.

Miranda, N.A., Baltazar, S., García, A., Munoz-Lira, D., Sepúlveda, P., Rubioa, M.A., Nicolas, D.A.F., 2016. Nanoscale zero valent supported by Zeolite and Montmorillonite: template effect of the removal of lead ion from an aqueous solution. J. Hazard. Mater. 301, 371–380.

Momcilovic, M., Purenovic, M., Bojic, A., Zarubica, A., Randelovic, M., 2011. Removal of lead(II) ions from aqueous solutions by adsorption onto pine cone activated carbon. Desalination 276, 53–59.

Musico, L.F., Santos, C.M., Dalida, M.L.P., Rodrigues, D.F., 2013. Improved removal of lead(II) from water using a polymer-based graphene oxide nanocomposite. J. Mater. Chem., 3789–3796

Park, S.K., Kim, K.D., Kim, H.T., 2002. Preparation of silica nanoparticles: determination of the optimal synthesis conditions for small and uniform particles. Colloids Surf. A Physicochem. Eng. Asp. 19, 7–17.

Rajput, M.S., Sharma, A.K., Sharma, S., Verma, S., 2015. Removal of Lead (II) from aqueous solutions by orange peel. Int. J. Appl. Res. 9, 411–413.

Saini, J., Garg, V.K., Gupta, R.K., 2018. Removal of Methylene Blue from aqueous solution by Fe_3O_4@Ag/SiO_2 nanospheres: synthesis, characterization and adsorption performance. J. Mol. Liq. 250, 413–422.

Sani, H.A., Ahmad, M.B., Hussein, M.Z., Brahim, N.A., Saleh, T.A., 2017. Nanocomposite of ZnO with montmorillonite for removal of

lead and copper ions.from aqueous solutions. Process Saf. Environ. Protect. 109, 97–105.
Shao, D., Chen, C., Wang, X., 2012. Application of polyaniline and multiwalled carbon nanotube magnetic composites for removal of Pb(II). Chem. Eng. J. 185–186, 144–150.
Theivasanthi, T., Alagar, M., 2013. Konjac bio-molecules assisted – rod/spherical shaped lead nano powder synthesized by electrolytic process and its characterization studies. Nano Biomed. Eng. 5, 11–19.
Thitame, P.V., Shukla, S.R., 2017. Removal of lead (II) from synthetic solution and industry wastewater using almond shell activated carbon. Environ. Prog. Sustain Energy 36, 1628–1633.
Wan, S., He, F., Wu, J., Wan, W., Gu, Y., Gao, B., 2016. Rapid and highly selective removal of lead from water using graphene oxide-hydrated manganese oxide nanocomposites. J. Hazard. Mater. 314, 32–40.
Weber, W., Morris, J., 1963. Kinetics of adsorption on carbon from solution. J. Sanit. Eng. Div. 89, 31–60.
Yang, S., Chen, C., Chen, Y., Li, J., Wang, D., Wang, X., Hu, W., 2014. Competitive adsorption of PbII, NiII, and SrII ions on graphene oxides: a combined experimental and theoretical study. ChemPlusChem 00, 1–5.
Yang, G., Tang, L., Zeng, G., Cai, Y., Tang, J., Pang, Y., Zhou, Y., 2015. Simultaneous removal of lead and phenol contamination from water by nitrogen-functionalized magnetic ordered mesoporous carbon. Chem. Eng. J. 259, 854–864.
Zhu, K., Chen, C., Xu, M., Chen, K., Tan, X., Wakeel, M., Alharbi, N.S., 2018. In-situ carbothermal reduction synthesis of Fe nanocrystals embedded into N-doped carbon nanospheres for highly efficient U(VI) adsorption and reduction. Chem. Eng. J. 331, 395–405.

Please cite this article in press as: Saini, J. et al., Green synthesized SiO_2@OPW nanocomposites for enhanced Lead (II) removal from water. Arabian Journal of Chemistry (2018), https://doi.org/10.1016/j.arabjc.2018.06.003